InterPore JOURNAL

Special Issue – Iran 2024
Original Research

OPTIMIZATION OF THE ENERGY EXTRACTION PROCESS FROM ENHANCED GEOTHERMAL SYSTEMS

Mohammad Norouzi Delaviz, Mozhdeh Sajjadi, Mohammad Emami Niri

Institute of Petroleum Engineering, School of Chemical Engineering, College of Engineering, University of Tehran, Tehran, Iran

Correspondence to:
Mozhdeh Sajjadi,
sajjadi.mozhdeh@ut.ac.ir

How to Cite:
Norouzi Delaviz, M., Sajjadi, M., & Emami Niri, M. (2026). Optimization of the Energy Extraction Process from Enhanced Geothermal Systems. *InterPore Journal*, *3*(1), IPJ010326-3. https://doi.org/10.69631/thzmfy53

RECEIVED: 23 May 2025
ACCEPTED: 11 Aug. 2025
PUBLISHED: 1 Mar. 2026

ABSTRACT

Enhanced Geothermal Systems (EGS) have emerged as a viable solution for sustainable energy extraction from hot dry rock reservoirs. In this study, numerical simulations are employed to investigate the optimization of energy extraction from enhanced geothermal systems, focusing on the effects of fracture geometry, the number of fractures, and well spacing on overall system performance and profitability. By validating the model against previously established semi-analytical and analytical models, this research explores the importance of the mentioned parameters in determining cumulative energy production and economic outcomes across different project lifespans. The results demonstrate that increased well spacing enhances energy output by delaying thermal breakthrough and increasing the optimal injection rates. Although small fractures have limited thermal capacity, the primary influence of fracture geometry is to limit the applicable distance between the wells. Deeper wells require more pumping power, which reduces net energy gain and lowers the optimal injection rate. Multiple fractures along the well enhance energy production, particularly at higher injection rates and for smaller fractures. Economic analyses underscore the importance of operational design (including the well placement and injection rate) in maximizing profitability.

KEYWORDS

Enhanced geothermal systems (EGS), Hydrothermal simulation, Finite fracture, Economic optimization, Hot dry rock (HDR), Heat transfer in porous media

1. INTRODUCTION

As global demand for clean and renewable energy continues to rise, there is a pressing need to further explore and evaluate the technical and economic viability of developing renewable energy resources (30). Geothermal energy offers a promising alternative to fossil fuels that can be used for domestic heating and reliable electricity production (6). The typical geothermal gradient of 25-30°C/Km provides a specific range of temperatures at depth, whereas in areas with high volcanic or tectonic activity, the gradient can be much steeper (around 50-70°C/Km). The utilization of the

extracted heat depends on the temperature of the produced water and may take the form of power generation or direct thermal use. Resources with low- to middle-range temperatures (below 150°C) may be developed using Ground Source Heat Pumps (GSHP) or Deep Bottom-hole Heat Exchangers (DBHE) (13). In contrast, higher geothermal gradients that yield bottom-hole temperatures above 150°C may justify the investment required for commercial power generation (17). **Figure 1** presents a simplified overview of the different source types of geothermal energy and their intended applications, based on the depth.

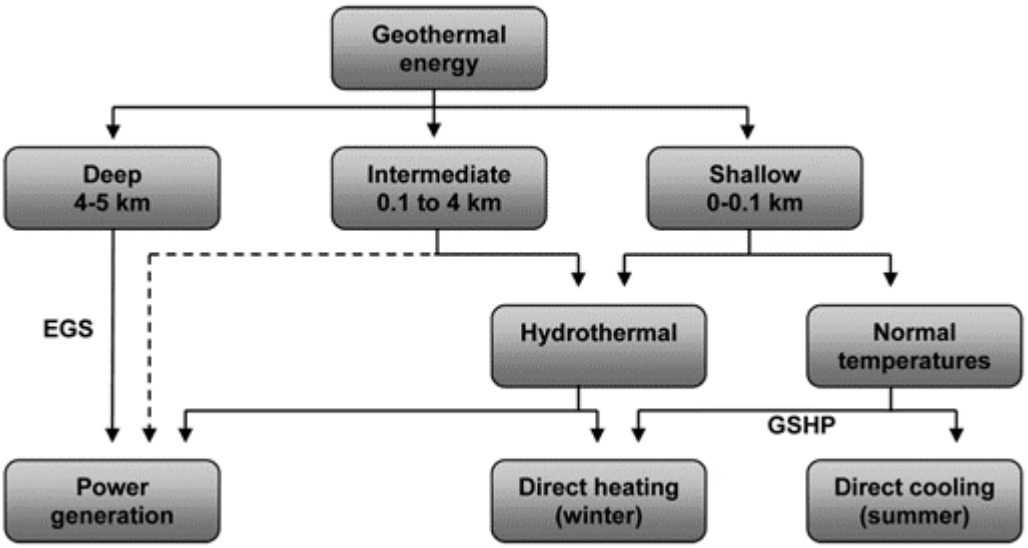

Figure 1: summary of the various methods for acquiring geothermal energy based on the depth of extraction and the intended applications (reproduced from (13)).

Deep geothermal resources may be divided into hydrothermal systems and enhanced geothermal systems (EGS) based on underground rock characteristics. Hydrothermal systems rely on high permeability and groundwater presence, while EGS extract heat from hot dry rock, necessitating artificial fracture creation for heat extraction. The technology for harnessing hydrothermal energy is relatively well established, with few remaining challenges, particularly in geotechnology (18). While hydrothermal energy remains a key contributor to the global renewable energy, its utilization is mostly confined to regions with water saturated porous formations. Conversely, EGS and Ground Source Heat Pump technologies are emerging with more abundant resources. Heat extraction from EGS is recognized as a promising technology for achieving long-term energy sustainability, thanks to their potential to significantly improve heat extraction from the Earth (7, 20). Yet despite notable progress in recent years, the commercial deployment of EGS remains limited (28) as their development is heavily reliant on geotechnological advancements. Nevertheless, they are poised to become more widespread and influential in future energy provision (13).

The construction of an EGS involves drilling injection and production wells, implementing hydraulic fracturing for reservoir creation, establishing a closed-loop fluid and heat transfer system, and enabling surface power generation through appropriate facilities (10). A simplified schematic of an EGS is illustrated in **Figure 2**.

The pioneering EGS site, Fenton Hill in New Mexico, established in 1974, confirmed the feasibility of hot dry rock exploration (12). Initially borrowing technologies from the oil and gas industry (22, 23), subsequent projects such as Rosemanowes (UK), Hijori (Japan), Fjällbacka (Sweden), and Ogachi (Japan) (29) , were later implemented (10). However, the high costs associated with these experimental projects limit their widespread implementation in many countries. Analytical models (25) and numerical simulations, by contrast, offer a cost-effective means of investigating a wide range of conditions (14). Nevertheless, numerical models are often unable to fully account for thermal-hydraulic-mechanical-chemical (THMC) interactions, realistically represent fracture networks, accurately model fluid-rock interactions, or robustly couple physical processes—capabilities that have been shown to be necessary for accurate estimation of the energy extraction performance.

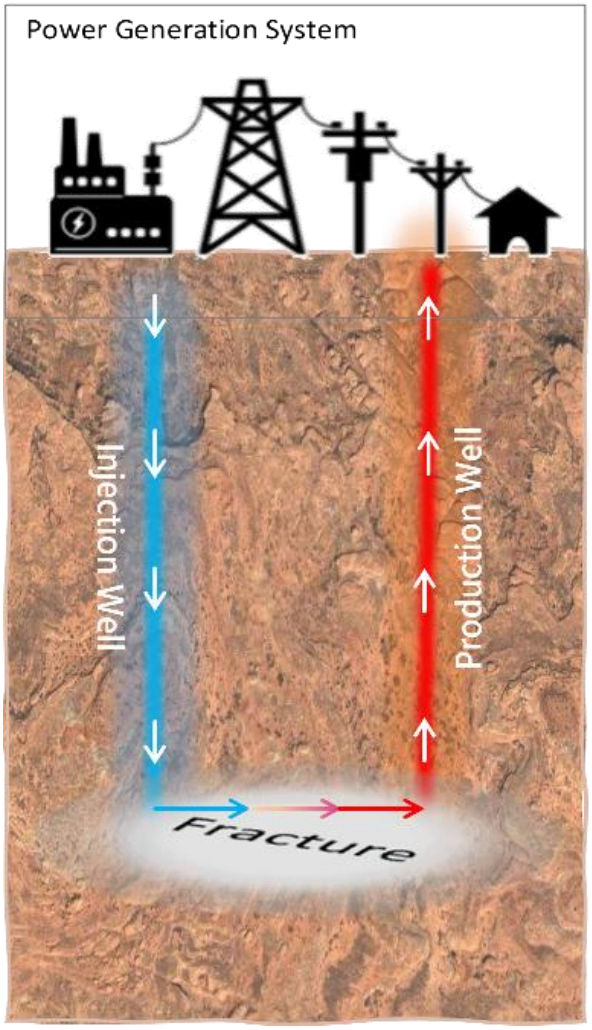

Figure 2: Schematic of an EGS consisting of injection and production wells and a fracture.

The performance of EGS is strongly influenced by local conditions, and economically viable energy extraction plants require accurate process design (26). Customized strategies aligned with different project stages require actual reservoir and process simulations (26). Therefore, various research efforts have been devoted to exploring performance prediction, sensitivity analysis, and optimization of EGS development systems. Kong et al. (15) presented a method for optimizing the placement of reinjection wells in geothermal reservoirs, aiming to sustain pressure and delay thermal breakthrough. By integrating numerical simulations and economic assessments, the research identified optimal well spacing. The techno-economic analysis of geothermal resources by Aljubran et al. (4) revealed that flexible operation could enhance profitability. Several studies have emphasized the necessity of suitable coupling between the essential operational factors, such as fracture spacing, well spacing, and flow rate, and the reservoir properties, such as rock permeability and geothermal gradient, to ensure project effectiveness (24, 27). These studies highlight the importance of finding the optimal well placement and operation design for each project.

The findings of previous studies on EGS energy extraction have uncovered optimized injection rates and well spacing for specific conditions, but the sensitivity of the optimization to the involved uncertainties has not been explored. This gap led us to propose a sensitivity analysis of the efficiency of this process with respect to different reservoir properties and operational parameters. The physical model of a simplified EGS system was built using COMSOL Multiphysics software[a]. In this manuscript, the effect of the fracture population and geometry, reservoir depth, and well spacing on the optimum injection rate leading to maximum cumulative energy extraction

[a] *https://www.comsol.com/*

over different operation times has been examined. Moreover, based on an economic analysis, the sensitivity of the revenue gained for each optimal scenario to the aforementioned parameters has been studied.

2. MODEL DESCRIPTION

The process of extracting heat from an EGS with a finite fracture involves heat transfer within the fracture and the surrounding rock via conduction and convection. Here, the fractures are characterized by flat circular openings of constant aperture. To examine the effect of fracture population, in addition to the single fracture model, scenarios with three fractures and five fractures have been envisaged. To reduce the calculation time, the system is assumed to be symmetric with respect to the middle fracture, and only the upper half of the system has been modeled. The extremely low reservoir permeability of $10^{-20}\ m^2\ (\sim 0.1\ \mu D)$ assigned to the modeled rock makes the surrounding formation effectively impermeable and prevents fluid leakage to the

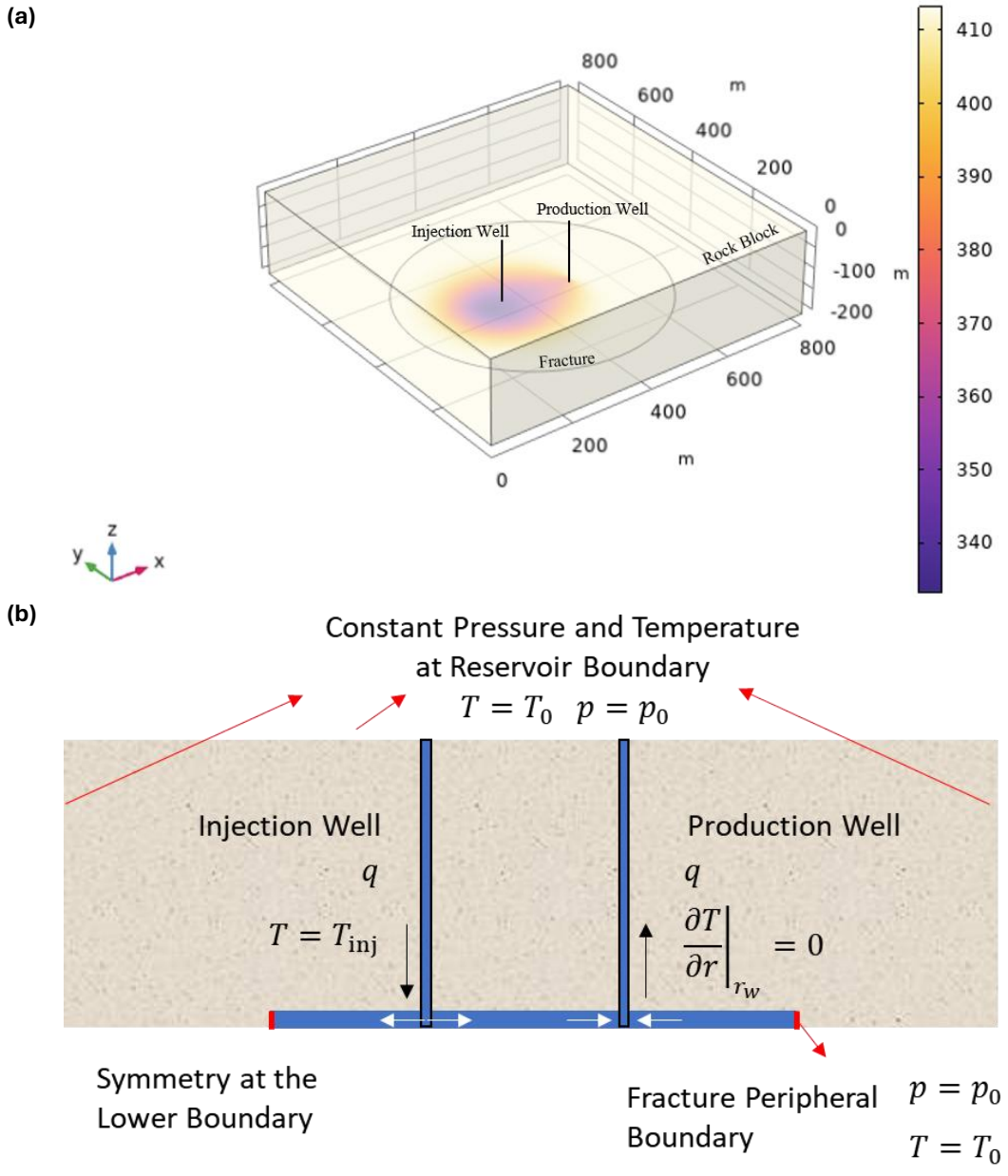

Figure 3: Schematic of an EGS with a single finite circular fracture: **(a)** the 3D rock block, fracture, and well doublet model built in COMSOL, **(b)** simplified 2D schematic with the applied boundary and initial conditions

 https://doi.org/10.69631/thzmfy53

overburden and underburden media. Additionally, the wells are assumed to be thermally isolated to prevent heat loss to the surrounding rock during transport to the surface facilities. Injection and production of water occur at constant rates. The schematics in **Figure 3** depict the reservoir fracture system.

3. GOVERNING EQUATIONS

The mathematical models that capture the dynamics of an EGS reservoir are based on the conservation laws of mass, energy, and momentum. This section outlines these equations in detail for both the rock matrix and the fracture system (2).

3.1. Flow Equations

The single-phase incompressible flow of water in the matrix is governed by the mass conservation equation, as given in **Equation 1** (3):

$$\frac{\partial}{\partial t}(\phi\rho_l) + \vec{\nabla}.(\rho_l\vec{u}) = Q_m \tag{1}$$

Here, ρ_l represents the fluid density, ϕ denotes the rock matrix porosity, $\vec{u}$ signifies Darcy's field velocity vector, and Q_m stands for the source term, which has a nonzero value only at the fracture surface, where $Q_m = -\frac{kA_e}{\mu V_e}\frac{\partial p}{\partial z}\Big|_{z_f}$ describes the water leakage from a fracture element, with surface area A_e, to the neighboring matrix element with volume V_e. z_f specifies the vertical location of each fracture. Darcy velocity is defined through Darcy's law (**Eq. 2**):

$$\vec{u} = -\frac{k}{\mu}\vec{\nabla}\mathrm{p} \tag{2}$$

This correlates the fluid velocity to its viscosity, μ, the rock's permeability, k, and the pressure gradient $\vec{\nabla}\mathrm{p}$. Likewise, the equation representing fluid flow within the fracture is expressed as (**Eq. 3**):

$$\frac{\partial}{\partial t}(\phi_f\rho_l) + \vec{\nabla}.(\rho_l\overrightarrow{u_f}) = -Q_m \tag{3}$$

where ϕ_f denotes the fracture porosity and $\overrightarrow{u_f}$ symbolizes the velocity within the fracture, expressed in (**Eq. 4**):

$$\overrightarrow{u_f} = -\frac{k_f}{\mu}\vec{\nabla}p_f \tag{4}$$

where k_f represents the fracture permeability, expressed as (**Eq. 5**; 1):

$$k_f = -\frac{d_f^2}{12f_f} \tag{5}$$

where d_f and f_f are the fracture's aperture and roughness factor, respectively. In this study, the value of f_f is assumed to be 1.

3.2. Heat Transfer Equations

The equations governing heat transfer in the porous rock are derived, assuming thermal equilibrium between the rock and the fluid (**Eq. 6**; 11**)**:

$$(\rho c_p)_{\mathrm{m,eff}}\frac{\partial T_m}{\partial t} + \rho_l c_{pl}\vec{u}.\vec{\nabla}T_m - K_{\mathrm{m,eff}}\nabla^2 T_m = \mathrm{Q} \tag{6}$$

where T_m denotes the matrix temperature, and c_{pl} signifies the specific heat capacity of the fluid. $(\rho c_p)_{\mathrm{m,eff}}$ and $K_{\mathrm{m,eff}}$ represent the effective heat capacity and thermal conductivity of the rock and fluid system, expressed in (**Eq. 7**, **Eq. 8**):

$$(\rho c_p)_{m,\mathrm{eff}} = \phi \rho_l c_{pl} + (1-\phi)\rho_m c_{pm} \tag{7}$$

$$K_{m,\mathrm{eff}} = \phi K_l + (1-\phi)K_m \tag{8}$$

where ρ_m and c_{pm} are the rock matrix density and specific heat capacity, respectively. K_m and K_l represent the thermal conductivities of the rock matrix and the fluid. At the fracture surface, the energy transferred to the fluid in the fracture is given by (**Eq. 9**):

$$Q = -\frac{A_e K_{\mathrm{m,eff}}}{V_e}\frac{\partial T}{\partial z}\Big|_{z_f} \tag{9}$$

At the rest of the rock block, this term is zero.

Likewise, the expression characterizing heat propagation in the fracture is presented in **Equation 10**:

$$(\rho c_p)_{\mathrm{f,eff}}\frac{\partial T_f}{\partial t} + \rho_l c_{pl}\overrightarrow{u_f}.\vec{\nabla}T_f + K_{\mathrm{f,eff}}\nabla^2 T_f = -\mathrm{Q} \tag{10}$$

where T_f denotes the fluid/rock temperature in the fracture, and $(\rho c_p)_{\mathrm{f,eff}}$ and $K_{\mathrm{f,eff}}$ represent the effective heat capacity and thermal conductivity of the rock and fluid system, expressed similarly to **Equations 7** and **8** by replacing the matrix porosity with the fracture porosity ϕ_f.

3.3. Initial and Boundary Conditions

The initial pressure in the rock is $p_0 = 10$ MPa. The reservoir is initially at 140°C (413.15 K). Although the intrinsic geothermal gradient implies a higher temperature at the lower rock block than the upper one, because the cooling of the rock only happens at a limited distance from the fractures, this difference may be neglected (25).

The pressure and temperature at the reservoir and fracture peripheral boundaries are assumed to remain constant throughout the simulation and are set equal to the initial pressure and temperature.

At the injection well, a constant flow rate at constant temperature is applied. The production well has a constant flow rate, equal to the injection rate, and the temperature gradient in the radial direction is held at zero, imposing an outlet boundary condition.

4. RESULTS AND DISCUSSION

The main aim of this study is to investigate the effect of fracture geometry and population, along with wellbore placement, on the optimum energy extraction conditions. The size of the circular fracture, as envisaged in this analysis, affects both the rock/fluid contact area and the maximum achievable distance between the injection and the production wells. The population of fractures in the fractured zone also affects the contact area available to the fluid. Here, the simulated scenarios quantify these effects in terms of the maximum extracted energy and the optimum injection rate. Therefore, the simulations have been performed for the described EGS for different values of fracture radius, well spacing, number of fractures, injection/production rate, and depth of the fractured zone, over 3-, 10- and 30-year life spans. The outlet temperature has been recorded as a function of time for each scenario for the validation of the simulation results, as well as for further calculation of the energy gain and economic analyses.

4.1. Model Validation

To validate the model, the simulation results have been verified against the study by Ghassemi et al. (9), which proposed a semi-analytical method to calculate the temperature distribution in the rock-fractures system. Their model geometry is similar to the single fracture model described so far. The flow rate, rock/fluid thermal properties, as well as the initial reservoir temperature and fracture geometry given in **Table 1** are adopted from Ghassemi et al. (9). The distance between the wells has been kept equal to the fracture radius. For the simulations, a wellbore radius of 2 cm has been defined. In **Figure 4**, the results obtained are compared with those of Ghassemi et al. (9) to confirm the accuracy and validity of the simulations. To comply with the original graphs of the paper, the dimensionless temperature $(T_{out} - T_{inj})/(T_0 - T_{inj})$ is plotted versus time for three fracture radii of 100, 150, and 200 m.

Table 1: Parameter values used for verifications and model presentation

Parameter	Symbol	Value
Rock thermal conductivity	K_r	2.58 W/m°K
Water density	ρ_l	1000 kg/m^3
Rock density	ρ_m	2650kg/m^3
Water heat capacity	c_{pl}	4050 J/kg K
Rock heat capacity	c_{pm}	1100 J/kg K
Initial reservoir temperature	T_0	140°C
Injection water temperature	T_{inj}	60°C
Injection and Production rates	q	0.005 $\frac{m^3}{s}$
Fracture aperture	d_f	1mm

The agreement between the models confirms the simulation's reliability in forecasting the production well's output temperature. There is a slight discrepancy between the simulation and the semi-analytical results, which is more significant initially but diminishes over time. It should be noted that Ghassemi et al. (9) modeled the production well as a point sink, while this study considers it with a finite radius, accounting for a non-uniform temperature distribution around the well. Therefore, the outlet temperature is defined as an average value in our models. The difference in this definition may be the cause of the discrepancy between the results.

The second part of validation compares the simulation results with the analytical solution for the outlet temperature in an EGS with a well doublet and an infinite horizontal fracture, proposed by Sajjadi et al. in (**Eq. 11**; 14):

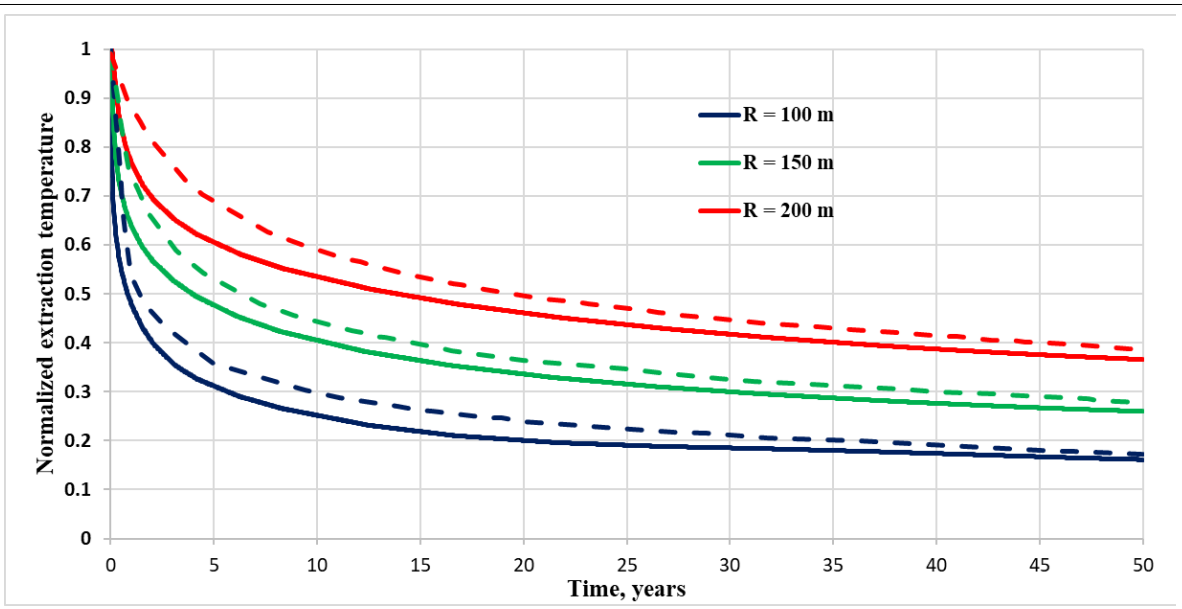

Figure 4: Production temperature in the simulations (solid lines), compared with the semi-analytical model by Ghassemi et al. (9) (dashed line). R is the fracture radius, and the rest of the model parameters are given in **Table 1**.

$$\frac{T_{out} - T_{inj}}{T_0 - T_{inj}} = \text{erf}\left(\frac{\frac{\pi K_m}{\rho_l c_{pl} q}\frac{D^2}{3}}{\sqrt{\lambda_r t}}\right) \quad (11)$$

with q describing the injection rate, D denoting the distance between the two wells, and $\lambda_r = \frac{K_r}{\rho_r c_r}$.

Figure 5 shows the comparison between the outlet temperature profiles for two well spacing values of 150 and 300 m, in two fractures with radii of 300 and 600 m, respectively. Two injection rates of 0.002 m^3/s and 0.004 m^3/s have been examined.

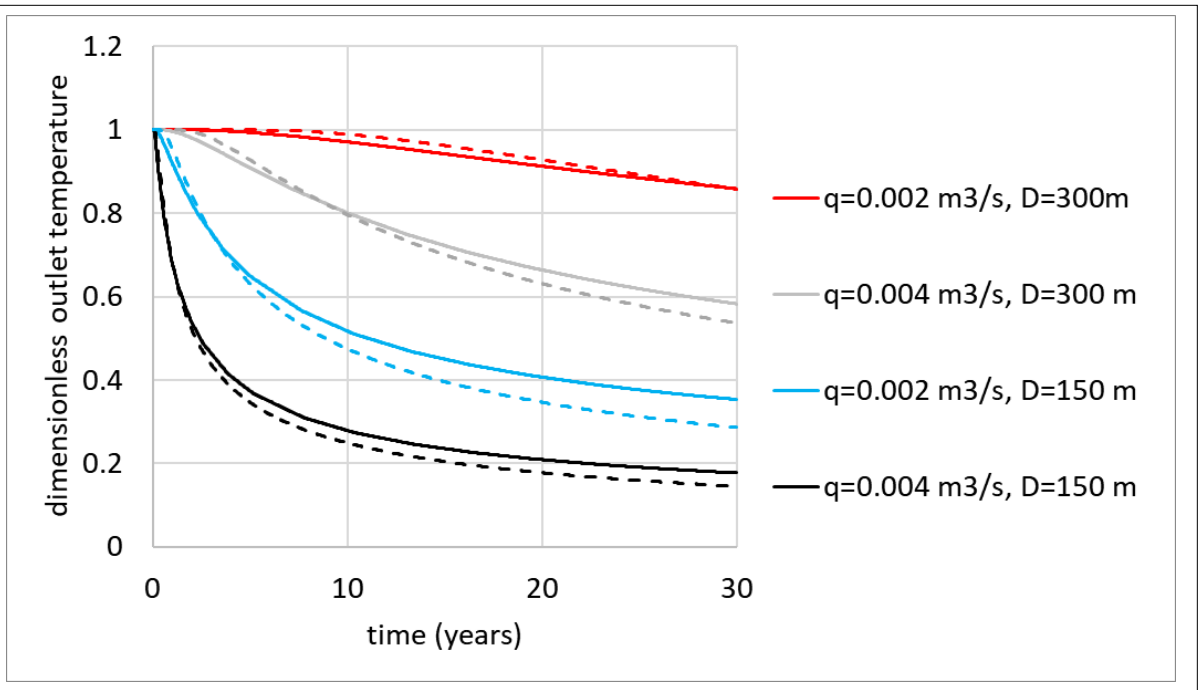

Figure 5: Analytically predicted outlet temperatures for a well doublet in an infinite fracture (solid lines), and the numerically calculated outlet temperatures for finite circular fractures (dashed lines). The radius of the fracture for the finite fracture scenarios is equal to the distance between the two wells.

The numerical simulation results are in good agreement with the analytical predictions, despite the difference in the infinite fracture dimensions and the simplifying assumptions in the analytical model. It should be noted that for this comparison, the temperature on the wellbore has been captured on the inner side, closer to the injection well.

4.2. Optimization and Sensitivity Analysis

In evaluating the economic feasibility of the development of EGS, our goal is to identify optimal injection and production rates that maximize cumulative energy production. In the simulations, the effects of fracture radius, the distance between the wells, the operational lifetime of the project, the well depth, and the number of fractures have been examined. Marginal parameters for the reservoir temperature (below 150°C), and well spacing (including values below 300 m), have been chosen to study the profitability of the relatively unfavorable scenarios. Since the energy production rate and the cumulative energy yield vary over time, the analysis has been conducted across three lifespans of 3, 10, and 30 years. The simulations have been conducted for fracture radii of 100, 200 and 300 m and well spacing ranging from 16 to 500 m, with wells symmetrically positioned around the center of the fracture. Optimal injection rates have been calculated for each scenario through a grid search process.

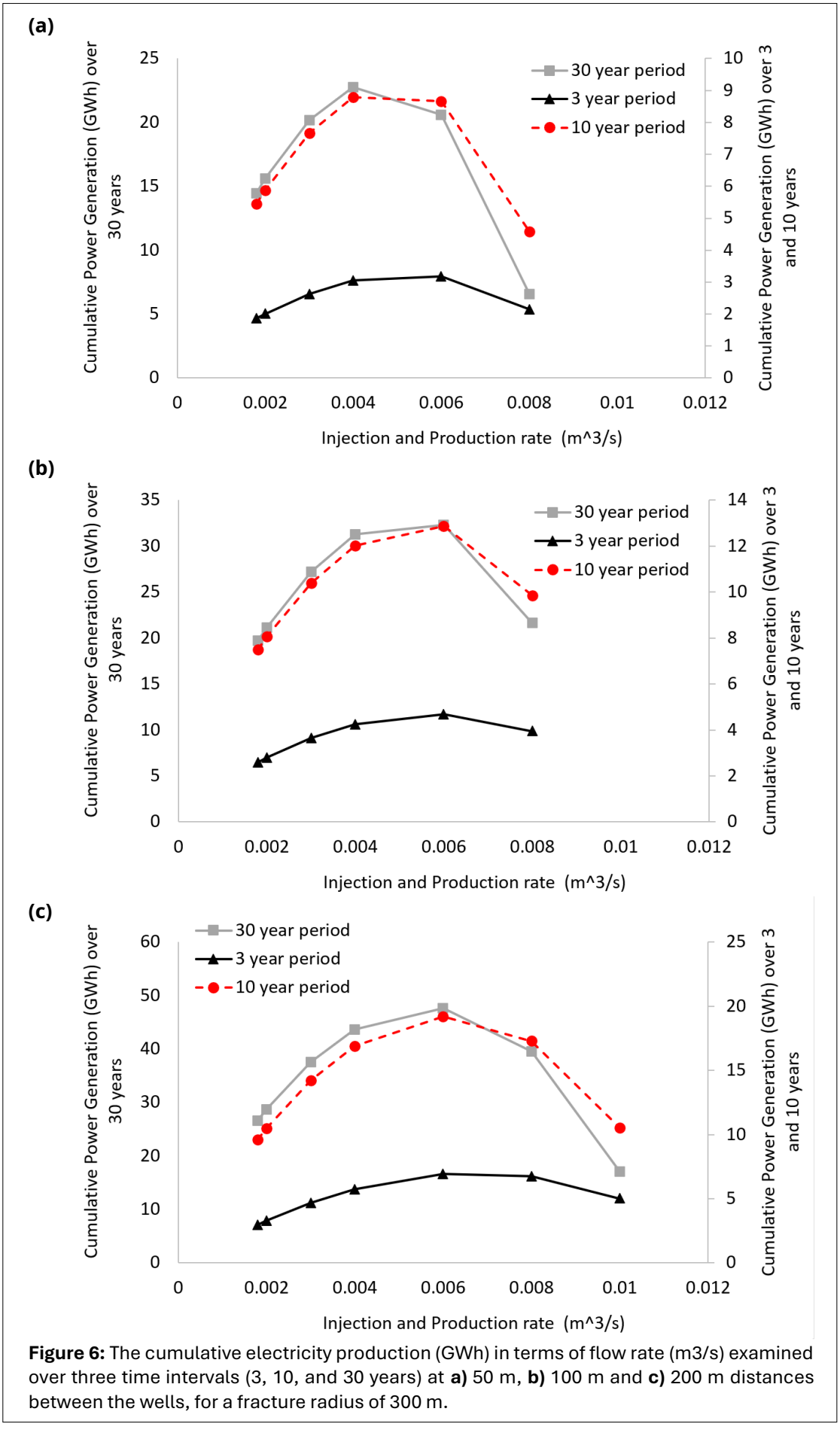

Figure 6: The cumulative electricity production (GWh) in terms of flow rate (m3/s) examined over three time intervals (3, 10, and 30 years) at **a)** 50 m, **b)** 100 m and **c)** 200 m distances between the wells, for a fracture radius of 300 m.

 https://doi.org/10.69631/thzmfy53

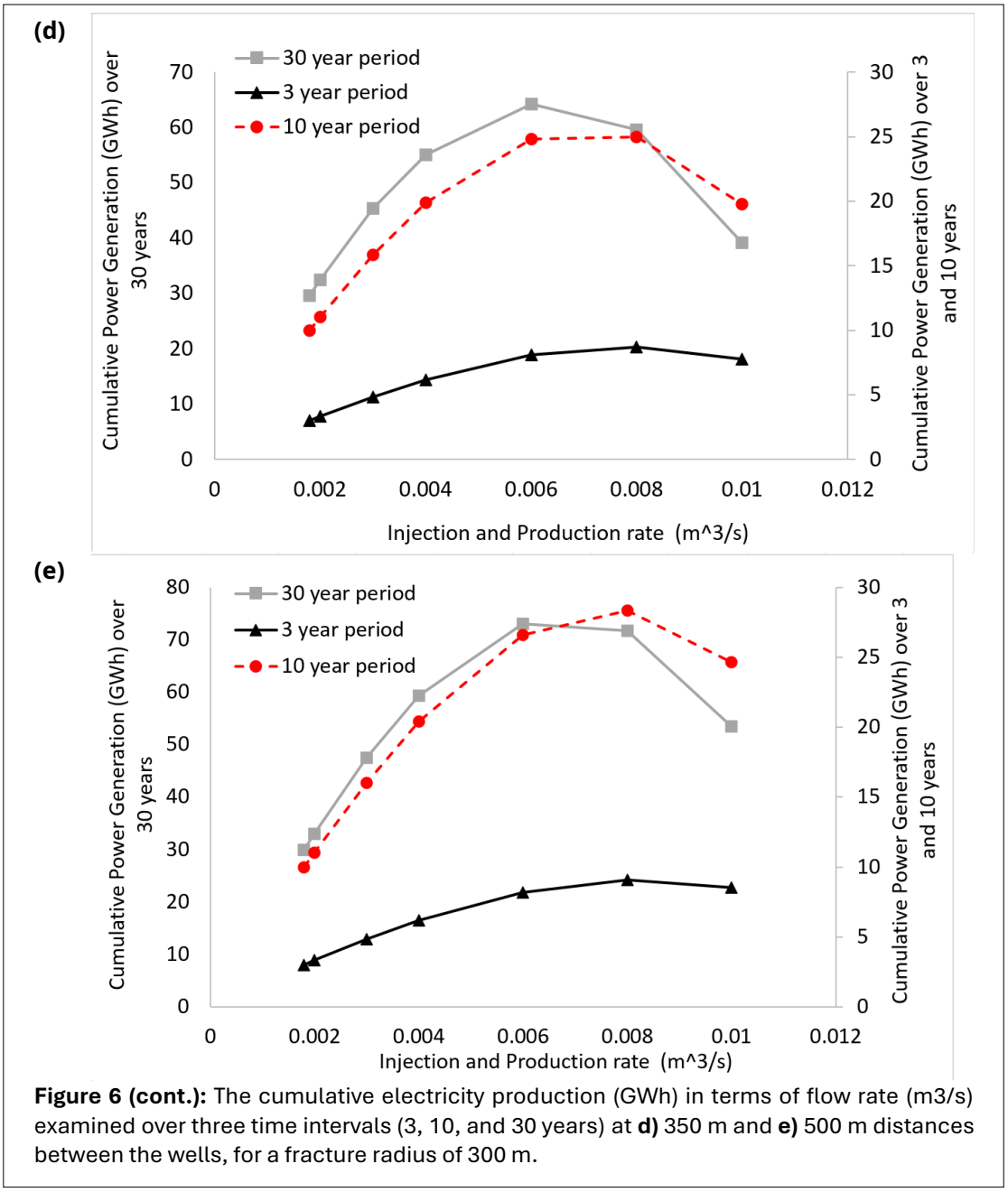

Figure 6 (cont.): The cumulative electricity production (GWh) in terms of flow rate (m3/s) examined over three time intervals (3, 10, and 30 years) at **d)** 350 m and **e)** 500 m distances between the wells, for a fracture radius of 300 m.

To study the influence of fracture size on the outlet temperature, initially, the scenarios were designed with the same aspect ratio between the well spacing and the fracture diameter, assuming that a proportional variation in the optimal conditions would be observed. However, further analysis showed that, regardless of the fracture size, the distance between the wells was the most influential factor in determining system's optimal conditions. As a result, in the next phase, the well distance was fixed, and the impact of fracture size on the cumulative energy production was evaluated independently.

Figure 6 presents graphs of net cumulative electricity production for different injection rates in a 300 m fracture at various production periods and well spacings. As a general trend, it is observed that increasing the injection rate initially boosts energy production, but it also speeds up thermal breakthrough at the production well, thereby reducing energy output over time. Therefore, for each scenario, there is an optimum injection rate that maximizes cumulative energy production. Over shorter periods, the benefit of higher production outweighs the impact of thermal

 https://doi.org/10.69631/thzmfy53

breakthrough, but as the operational time extends, delaying breakthrough becomes increasingly advantageous. Thus, for short-term planning, a higher optimal injection rate maximizes energy output.

Increasing the distance between the wells delays thermal breakthrough; thus, the optimal injection rate rises as wells are spaced farther apart, boosting the system's production capacity. Although a wider distance between the wells implies a higher pressure drop between the wells, and is not favorable for net energy production, in the range of values tested here, it never surpasses the advantage of delayed breakthrough time and higher production rates. Therefore, based on our analyses, the farther the wells are placed, the higher the energy gain.

For a 300 m fracture radius over three years, the net energy production can range from 2 to 10 GWh, emphasizing the importance of accurate predictions and optimal design of the extraction process. Depending on the well placement and the injection rate, this range may reach 5–30 GWh over 10 years and 5–70 GWh over 30 years. Optimal injection rates across the tested distances and lifespans that provide the maximum net energy production range between 0.004 m^3/s and 0.008 m^3/s.

Similar examinations of the optimal injection rate over different project life spans have been conducted for 200 m and 100 m fractures as well. However, for brevity, we skip the detailed graphs and only report the general trends. Reducing the fracture radius limits the applicable distance between the wells, hence limiting the range of cumulative energy production values. Additionally, the system's sensitivity to energy extraction time increases for shorter well distances. These observations highlight that understanding the fractured zone's dimensions and adjusting injection and production rates based on the planned production period are essential for maximizing the system's net energy output.

Given the substantial impact that the distance between wells has on the performance of EGS, the effect of fracture size has been isolated from that of the well spacing. For this purpose, the optimal injection rates for three fracture radii, 300, 200, and 100 m, have been sought while keeping the well spacing constant at 50 m. The results of this analysis, conducted over both 3- and 30-year

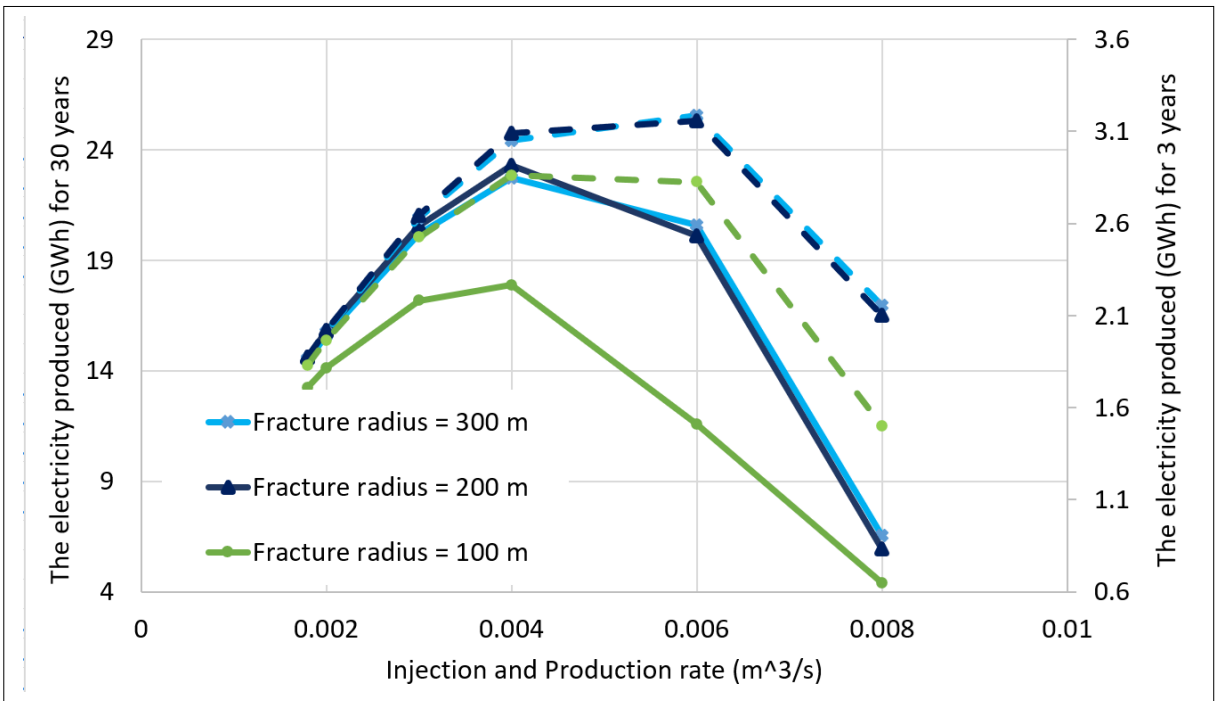

Figure 7: The effect of fracture size on cumulative electricity production over 3 years (dashed lines) and 30 years (solid lines).

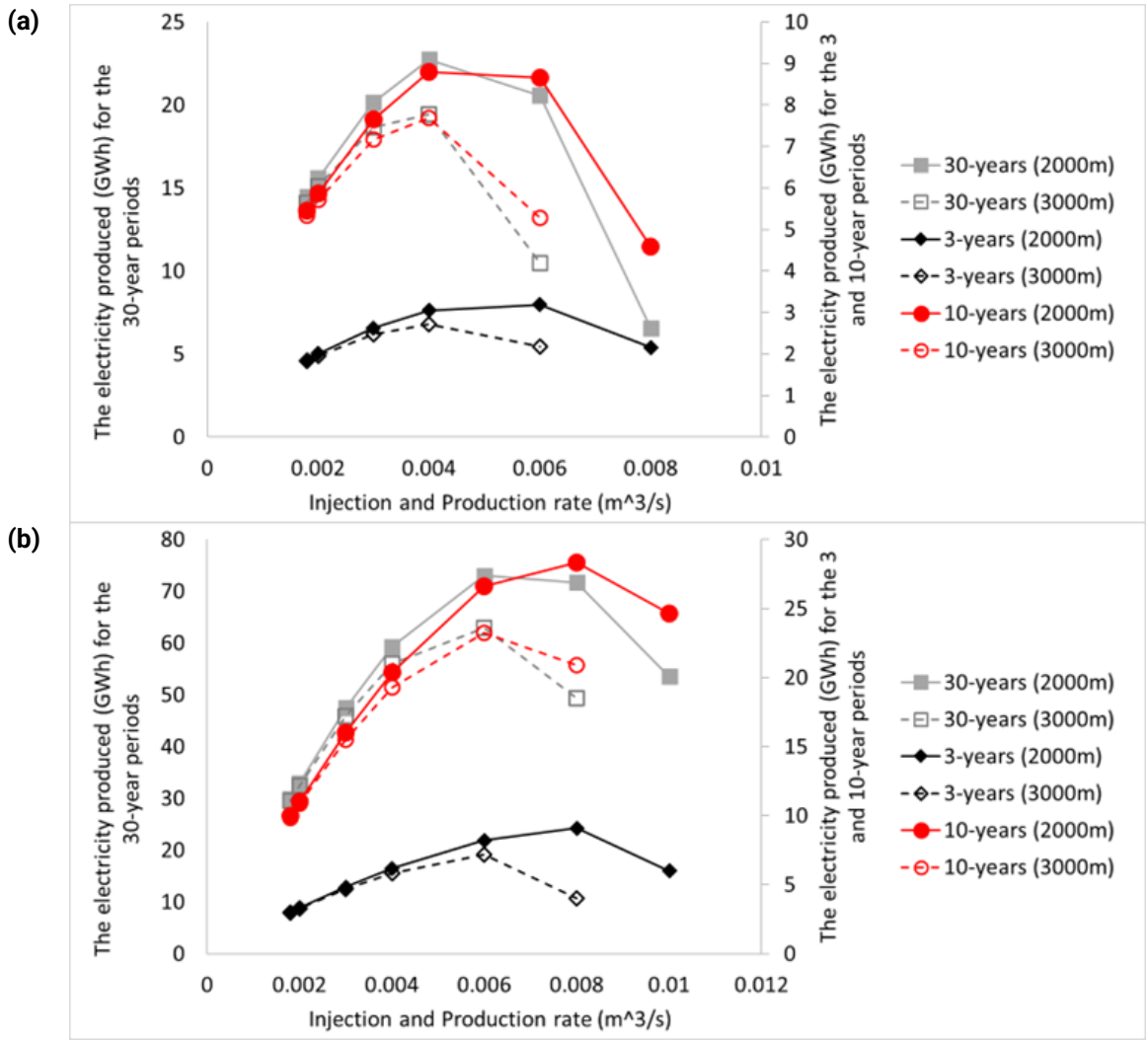

Figure 8: The effect of well depth on electricity production (GWh) over three time periods (3, 10, and 30 years) at **(a)** 50 m and **(b)** 500 m well spacing, for a fracture radius of 300 m.

periods, are presented in **Figure 7**. The graphs reveal that the influence of fracture size is particularly significant for smaller radii, especially over longer operational periods. At fracture radii of 300 and 200 m, cumulative energy production remains unchanged, with the optimal injection rate consistently occurring at 0.006 m^3/s across both the 3- and 30-year periods. However, by reducing the fracture radius to 100 m, cumulative energy production declines, and the optimal injection rate reduces to 0.004 m^3/s over the 30-year period. This suggests that smaller fractures lose more heat over time, necessitating a lower injection rate for sustained energy extraction. Additionally, based on the similarity between the curves for 200 m and 300 m fractures, it can be concluded that while larger fracture sizes in hydraulic fracturing for EGS systems facilitate greater well spacing and increase the surface area available for heat extraction, they do not necessarily result in higher energy production when well spacing is fixed.

In EGS, well depth is a critical factor that directly impacts the system's performance. Enhanced geothermal systems are mostly developed at depths of 3 to 5 km. As the well depth increases, the fluid encounters more resistance along its path to the surface, requiring greater pumping power to overcome this resistance. This pressure drop can reduce energy output and indirectly affect the optimal injection rate. To investigate this effect, the well depth has been changed to 3000 m, assuming a different geothermal gradient and keeping the reservoir temperature the same as in the 2000 m wells.

 https://doi.org/10.69631/thzmfy53

Figure 8 compares the effects of well depth on cumulative electricity generation for the scenarios depicted in **Figures 6a** and **6e**. The cumulative energy production curves show a shift in the optimal injection rate towards lower values for deeper wells. Another observed difference is in cumulative energy production, which is about 20% to 25% lower for the deeper wells. Over extended operational periods, and at wider distances between the wells, where higher injection rates are feasible, the gap between cumulative electricity production curves becomes more evident.

Multi-stage fracturing can enhance the contact area between the hot dry rock and the fluid. To study the effect of the number of fractures on the optimal conditions and the generated electricity, two systems with three and five fractures, positioned 50 m apart symmetrically above and below the initial fracture, have been modelled. The injection rate is divided equally between the fractures. **Figure 9** shows the comparison between single-fracture and multi-fracture systems for two well spacings of **(a)** 50 m and **(b)** 500 m in a 300 m radius fracture.

According to the graphs in **Figure 9**, for the same injection rate, more fractures yield higher cumulative energy, especially at higher injection rates. At lower rates, extra fractures do not

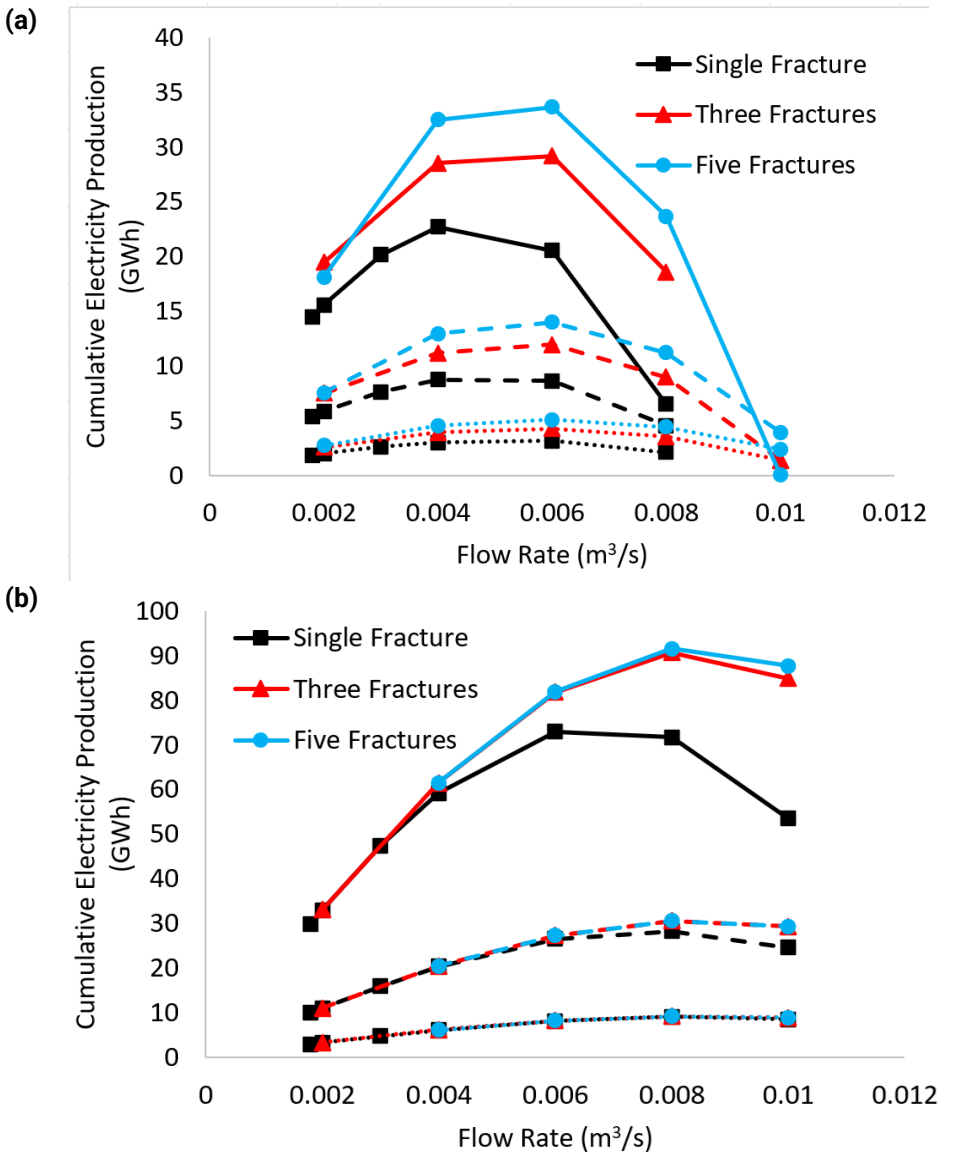

Figure 9: The effect of the number of fractures on net electricity production (GWh) over 3 years (dotted lines), 10 years (dashed lines), and 30 years (solid lines) of operation at **(a)** 50 m and **(b)** 500 m well spacing, for fracture radii of 300 m.

 https://doi.org/10.69631/thzmfy53

improve efficiency as much, since heat extraction is already efficient. For the same reason, the benefit of more fractures amplifies when the wells are closer to each other, but this advantage fades with greater distances. The cooling effect overlaps in the area between the fractures; thus, the optimum flow rate and the energy gained are not enhanced proportionally to the number of fractures. Full development of the cool zone in scenarios with wider distances between the wells causes the five-fracture system to not show much improvement over the three-fracture system in **Figure 9b**. **Table 2** shows the percen-tage of energy gain from additional fractures at optimal flow rates compared to a single fracture.

Table 2: Percentage of improvement in cumulative energy production relative to the single fracture system achieved by increasing the number of fractures.

Spacing	**50 m**		**500 m**	
Operational Time	**3 Fractures**	**5 Fractures**	**3 Fractures**	**5 Fractures**
3 years	35%	61%	2%	2%
10 years	36%	59%	8%	8%
30 years	28%	48%	24%	25%

In real field cases, there is a complex network of fractures available to the flow. Also, it is customary to explore higher reservoir temperatures (above 150°C) and apply wider distances between the wells. Therefore, injection and production rates almost an order of magnitude higher than the rates we used in our simulations are employed by the industry. Despite these differences, the trends and the role of parameters are similar between the simplified models and real field applications. As a summary of the conducted sensitivity analysis, a heatmap showing the sensitivity of the optimum flow rate and the cumulative energy production to the varied features, i.e. well spacing, well depth, and the number of fractures, is illustrated in **Figure 10**. The fracture diameter has been omitted from the analysis due to its correlation with the distance between the wells. The heatmap vividly demonstrates the strong impact of well spacing and flow rate on the

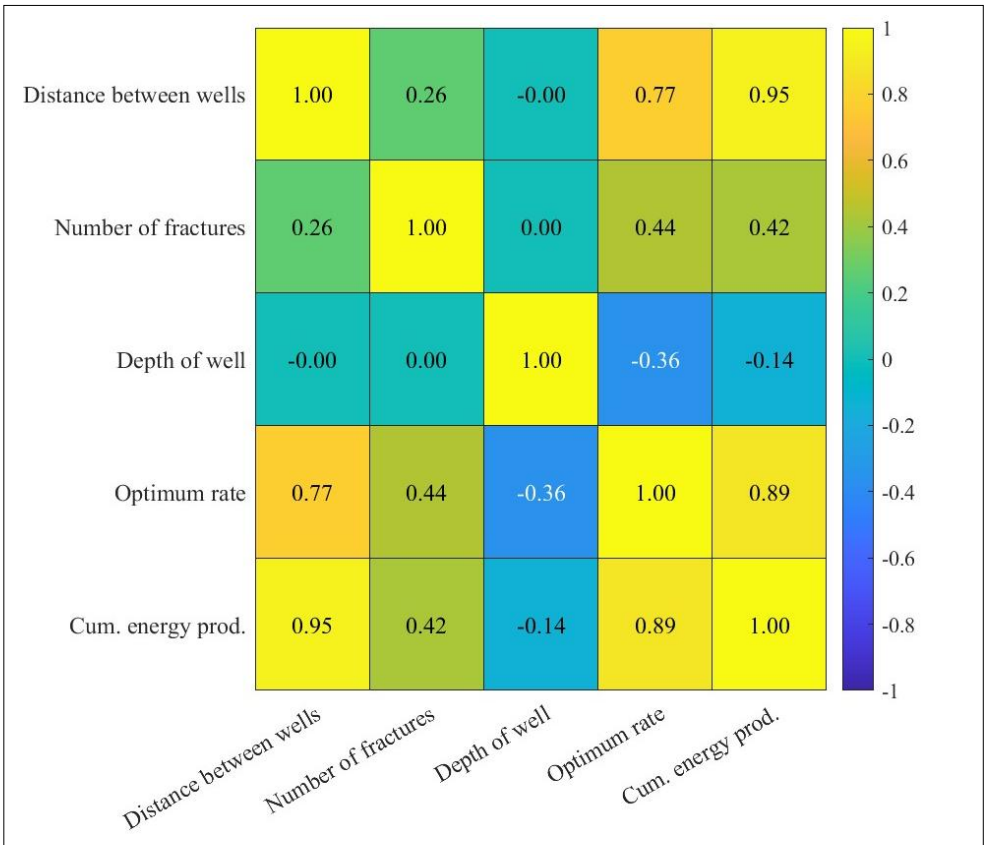

Figure 10: The heatmap of the correlation between the optimum flow rate and the 30-year cumulative energy production and the analyzed parameters.

cumulative energy production. The distance between the wells is the most important parameter in determining the optimum flow rate. The number of fractures has a moderate yet considerable effect on both output features. The well depth has the least significant effect with a negative correlation with both the optimum flow rate and the cumulative energy production.

4.3. Economic Study

Enhanced geothermal system projects demand rigorous economic analysis to support secure investment decisions. Assessing the costs and potential profitability of these projects is essential for determining the viability of scaling up of this technology. The feasibility of the energy extraction system is assessed through examination of the maximum profit gained over 3, 10, and 30 years of operation. For this analysis, the initial capital investment for drilling, piping, and installing the power plant is assumed to be fixed for the different scenarios examined. Therefore, it does not influence the optimal condition evaluation. For the operational cost, the cost of electricity required for pumping the fluid has been considered, and the revenue is from the electricity produced from the recovered heat at the surface.

The cost of electricity used for pumping the fluid into the well and up to the surface over the ith time step Δt may be calculated as follows (**Eq. 12**):

$$C_{P_i} = \frac{q\Delta P_i}{\eta_p}\Delta t.pp \tag{12}$$

Here, ΔP is the pressure difference between the injection and the production points at the surface at the ith time step, and η_p is the efficiency of the pump. The simulation results are extracted at a time step size of $\Delta t = 0.02$ years. pp is the rate of electricity in \$/KWh.

To calculate the pressure difference between the injection and the production points, the pressure drop inside each well as well as the pressure drop between the injection and the production points in the fracture have been considered (**Eq. 13**):

$$\Delta P = \Delta P_{\text{fracture}} + 2\Delta P_{\text{wellbore}} \tag{13}$$

The pressure distribution in the fracture is obtained from the simulations. The pressure drop in the wells depends on the friction factor, $f_{D,}$ calculated based on the flow's Reynolds number, $Re = \frac{\rho_l V d}{\mu}$. For the range of injection rates used in this study, the pressure drop may be obtained from (**Eq. 14**, **Eq. 15**; 16):

$$\Delta P_{\text{wellbore}} = \rho_f g h_f \tag{14}$$

$$h_f = f_D \frac{LV^2}{4r_w g} \tag{15}$$

In this context, $V = \frac{q}{\pi r_w^2}$ represents the fluid velocity inside the well of radius r_w, and length L. For the economic analysis, the fluid viscosity has been averaged between the temperatures at the surface and the bottom of the well. Finally, the friction factor is determined using (**Eq. 16**; 5):

$$f_D = (100 * \text{Re})^{-\frac{1}{4}} \tag{16}$$

The expected outlet temperature range of 80–130°C, falls within the range of application of Organic Rankin Cycle (ORC) powerplants for electric energy generation. These cycles are known for their flexibility in design for different heat source temperatures, and capacities (19). Thus, the revenue from the electricity produced over the ith time step is obtained from (**Eq. 17**):

$$C_{T_i} = \rho_l c_{pl} q (T - T_{inj})_i \, \eta_R \Delta t . pp \quad (17)$$

Here η_R is the efficiency of the ORC plant, assumed to be 0.2 for the obtained range of outlet temperatures (21). The cumulative profit over N years of operation is determined over the lifespan of the projects by integrating the subtraction of the cost from the revenue over $n = N/\Delta t$ time steps. The net profit of the EGS plant, accounting for the annual inflation rate r may be calculated as follows (**Eq. 18**; 15, 25):

$$\mathrm{C} = \sum_{i=0}^{n} \frac{(C_T + C_p)_i}{(1 + r\Delta t)^i} = \sum_{i=0}^{n} \frac{\left(\rho_f c_f q \left(T - T_{inj}\right)_i \eta_R \Delta t - \left(P_{inj} - P_{prod}\right)_i q/\eta_p \Delta t\right) . pp}{(1 + r\Delta t)^i} \quad (18)$$

The term $r\Delta t$ corrects the annual inflation rate over the time step Δt, expressed as a fraction of a year. The cumulative and annual average profits at optimal flow rates across varying fracture radii and inter-well distances have been calculated and reported in **Table 3**, **Table 4**, and **Table 5** for different fracture sizes. The annual inflation rate has been fixed at $r = 5\%$ over the project lifespan studied. For our analyses, the average cost of electricity is 0.289 Euros per KWh (8).

The results indicate that increasing the distance between the wells and access to larger fractures results in higher achievable cumulative and average annual profits. The projects have higher return rates in the initial years; therefore, increasing the operational life of the projects reduces their average annual income. The average annual income over 30 years for large fractures is almost half of the average annual income in the first three years. The ratio is reduced for smaller fractures due to their limited capacity. These insights highlight the need for precise simulation and optimization of energy extraction processes in EGS based on the investment cost and the in situ conditions. With careful optimization and modeling, both energy efficiency and economic returns can be substantially improved.

Table 3: Net profit from electricity production (in million Euros) and average annual profit over the lifespan of the project (in million Euros per year), from a 300 m fracture.

Well Spacing (m)	Time (years)	Opt. Rate (m^3/s)	Cum.	Ave.
50	3	0.006	0.85	0.28
	10	0.004	2.02	0.20
	30	0.004	3.66	0.12
100	3	0.006	1.26	0.42
	10	0.006	3.04	0.30
	30	0.006	5.60	0.19
200	3	0.006	1.84	0.61
	10	0.006	4.46	0.45
	30	0.006	8.13	0.27
350	3	0.006	2.34	0.45
	10	0.004	5.82	0.58
	30	0.004	10.4	0.35
500	3	0.008	2.42	0.81
	10	0.008	6.54	0.65
	30	0.006	12.3	0.41

 https://doi.org/10.69631/thzmfy53

Table 4: Net profit from electricity production (in million Euros) and average annual profit over the lifespan of the project (in million Euros per year), from a 200 m fracture.

Well Spacing (m)	Time (years)	Opt. Rate (m^3/s)	Cum.	Ave.
33.3	3	0.004	0.70	0.23
	10	0.004	1.72	0.17
	30	0.004	3.20	0.11
66.66	3	0.006	1.00	0.33
	10	0.006	2.30	0.23
	30	0.004	4.10	0.14
133.33	3	0.006	1.45	0.48
	10	0.006	3.34	0.33
	30	0.004	5.83	0.19
233.33	3	0.006	1.92	0.64
	10	0.006	4.60	0.46
	30	0.006	8.00	0.27
333.33	3	0.008	2.10	0.7
	10	0.006	5.24	0.52
	30	0.006	9.26	0.31

Table 5: Net profit from electricity production (in million Euros) and average annual profit over the lifespan of the project (in million Euros per year), from a 100 m fracture.

Well Spacing (m)	Time (years)	Opt. Rate (m^3/s)	Cum.	Ave.
16.66	3	0.004	0.52	0.17
	10	0.004	1.22	0.12
	30	0.003	2.13	0.07
33.33	3	0.004	0.67	0.22
	10	0.004	1.60	0.16
	30	0.004	2.80	0.09
66.66	3	0.004	0.86	0.29
	10	0.004	2.02	0.20
	30	0.004	3.50	0.12
116.66	3	0.006	1.08	0.36
	10	0.004	2.40	0.24
	30	0.004	3.94	0.13
166.66	3	0.006	1.22	0.41
	10	0.004	2.64	0.26
	30	0.004	4.26	0.14

5. CONCLUSION

This study examined the effect of fracture geometry and population, well spacing, and well depth, on the optimal operational conditions and economic gains of doublet well EGS systems. Through numerical simulations and sensitivity analyses, it was found that for a fixed well spacing (here, 50 m) a larger fracture size has only a modest impact of around 5% on the total energy output for the explored fractures of 100, 200, and 300 m radii. Increasing well spacing leads to higher optimal injection rates, which, in turn, boosts cumulative energy production. Pumping the water in a 3000 m well instead of a 2000 m well reduces the maximum achievable production by 20-25% depending on the wellbore spacing and operational time. Shorter spacing between the wells can be compensated for by increasing the number of fractured zones along the well. A five-fracture

system, for instance, leads to 50-60% more energy production (depending on the operation time) compared to a single-fracture system when the wells are 50 m apart. The leverage is less significant when the wells are placed farther apart.

Economic analysis of EGS revealed that optimal profitability in these systems is strongly affected by both the distance between the wells and the operational period. While longer energy extraction periods yield larger cumulative returns, shorter operational periods show higher average annual income.

STATEMENTS AND DECLARATIONS

Author Contributions

M. N. Delaviz: Formal analysis, Investigation, Data curation, Visualization, Validation, Writing - Original Draft. **M. Sajjadi:** Conceptualization, Methodology, Resources, Supervision, Validation, Writing – Review & Editing. **M. E. Niri:** Project administration, Supervision, Writing – Review & Editing.

Conflicts of Interest

The authors declare that there is no conflict of interest influencing this research or publication of this paper.

ORCID IDs

Mohammad Norouzi Delaviz https://orcid.org/0009-0004-1295-3738
Mozhdeh Sajjadi https://orcid.org/0000-0002-8626-2153
Mohammad Emami Niri https://orcid.org/0000-0002-4814-1289

REFERENCES

1. Aliyu, M. D., & Chen, H.-P. (2018). Enhanced geothermal system modelling with multiple pore media: Thermo-hydraulic coupled processes. Energy, 165, 931–948. https://doi.org/10.1016/j.energy.2018.09.129
2. Aliyu, M. D., Finkbeiner, T., Chen, H.-P., & Archer, R. A. (2023). A three-dimensional investigation of the thermoelastic effect in an enhanced geothermal system reservoir. *Energy*, *262*, Article 125466. https://doi.org/10.1016/j.energy.2022.125466
3. Aliyu, M. D. et al. Numerical modelling of geothermal reservoirs with multiple pore media. In Proceedings of the 42nd Workshop on Geothermal Reservoir Engineering Stanford University, Stanford, CA. 2017.
4. Aljubran, M. J., & Horne, R. N. (2025). Techno-economics of geothermal power in the contiguous United States under baseload and flexible operations. *Renewable and Sustainable Energy Reviews*, *211*, Article 115322. https://doi.org/10.1016/j.rser.2024.115322
5. Arbhabhirama, A., & Dinoy, A. A. (1973). Friction factor and Reynolds number in porous media flow. *Journal of the Hydraulics Division*, *99*(6), 901–911. https://doi.org/10.1061/JYCEAJ.0003663
6. Bayer, P., Rybach, L., Blum, P., & Brauchler, R. (2013). Review on life cycle environmental effects of geothermal power generation. *Renewable and Sustainable Energy Reviews*, *26*, 446–463. https://doi.org/10.1016/j.rser.2013.05.039
7. Cheng, Y., Zhang, Y., Yu, Z., Hu, Z., & Yang, Y. (2020). An investigation on hydraulic fracturing characteristics in granite geothermal reservoir. *Engineering Fracture Mechanics*, *237*, Article 107252. https://doi.org/10.1016/j.engfracmech.2020.107252
8. Electricity price statistics. Eurostat. Retrieved July 1, 2025, https://ec.europa.eu/eurostat/statistics-explained/index.php?title=Electricity_price_statistics
9. Ghassemi, A., Tarasovs, S., & Cheng, A. H.-D. (2003). An integral equation solution for three-dimensional heat extraction from planar fracture in hot dry rock. *International Journal for Numerical and Analytical Methods in Geomechanics*, *27*(12), 989–1004. https://doi.org/10.1002/nag.308

10. Gao, X., Li, T., Zhang, Y., Kong, X., & Meng, N. (2022). A review of simulation models of heat extraction for a geothermal reservoir in an enhanced geothermal system. *Energies*, *15*(19), 7148. https://doi.org/10.3390/en15197148
11. Guo, T., Gong, F., Wang, X., Lin, Q., Qu, Z., & Zhang, W. (2019). Performance of enhanced geothermal system (EGS) in fractured geothermal reservoirs with CO_2 as working fluid. *Applied Thermal Engineering*, *152*, 215–230. https://doi.org/10.1016/j.applthermaleng.2019.02.024
12. He, R., Rong, G., Tan, J., Phoon, K.-K., & Quan, J. (2022). Numerical evaluation of heat extraction performance in enhanced geothermal system considering rough-walled fractures. *Renewable Energy*, *188*, 524–544. https://doi.org/10.1016/j.renene.2022.02.067
13. Johnston, I. W., Narsilio, G. A., & Colls, S. (2011). Emerging geothermal energy technologies. *KSCE Journal of Civil Engineering*, *15*(4), 643–653. https://doi.org/10.1007/s12205-011-0005-7
14. Keçebaş, A. (2011). Performance and thermo-economic assessments of geothermal district heating system: A case study in Afyon, Turkey. *Renewable Energy*, *36*(1), 77–83. https://doi.org/10.1016/j.renene.2010.05.022
15. Kong, Y., Pang, Z., Shao, H., & Kolditz, O. (2017). Optimization of well-doublet placement in geothermal reservoirs using numerical simulation and economic analysis. *Environmental Earth Sciences*, *76*(3), 1–7. https://doi.org/10.1007/s12665-017-6404-4
16. Li, H., Lu, Y., Peng, X., Lv, X., & Wang, L. (2016). Pressure drop calculation models of wellbore fluid in perforated completion horizontal wells. *International Journal of Heat and Technology*, *34*(1), 65–72. https://doi.org/10.18280/ijht.340110
17. Li, K., Bian, H., Liu, C., Zhang, D., & Yang, Y. (2015). Comparison of geothermal with solar and wind power generation systems. *Renewable and Sustainable Energy Reviews*, *42*, 1464–1474. https://doi.org/10.1016/j.rser.2014.10.049
18. Liu, G., Yuan, Z., Zhou, C., Fu, Z., Rao, Z., & Liao, S. (2023). Heat extraction of enhanced geothermal system: Impacts of fracture topological complexities. *Applied Thermal Engineering*, *219*, Article 119236. https://doi.org/10.1016/j.applthermaleng.2022.119236
19. Liu, X., Falcone, G., & Alimonti, C. (2018). A systematic study of harnessing low-temperature geothermal energy from oil and gas reservoirs. *Energy*, *142*, 346–355. https://doi.org/10.1016/j.energy.2017.10.058
20. Liu, Z., Wu, M., Zhou, H., Chen, L., & Wang, X. (2024). Performance evaluation of enhanced geothermal systems with intermittent thermal extraction for sustainable energy production. *Journal of Cleaner Production*, *434*, Article 139954. https://doi.org/10.1016/j.jclepro.2023.139954
21. Lu, S.-M. (2018). A global review of enhanced geothermal system (EGS). *Renewable and Sustainable Energy Reviews*, *81*, 2902–2921. https://doi.org/10.1016/j.rser.2017.06.097
22. Mahmoodpour, S., Singh, M., Bär, K., & Sass, I. (2022b). Thermo-hydro-mechanical modeling of an enhanced geothermal system in a fractured reservoir using carbon dioxide as heat transmission fluid-A sensitivity investigation. *Energy*, *254*, Article 124266. https://doi.org/10.1016/j.energy.2022.124266
23. Mahmoodpour, S., Singh, M., Turan, A., Bär, K., & Sass, I. (2022a). Simulations and global sensitivity analysis of the thermo-hydraulic-mechanical processes in a fractured geothermal reservoir. *Energy*, *247*, Article 123511. https://doi.org/10.1016/j.energy.2022.123511
24. Pandey, S. N., & Vishal, V. (2017). Sensitivity analysis of coupled processes and parameters on the performance of enhanced geothermal systems. *Scientific Reports*, *7*(1), Article 17057. https://doi.org/10.1038/s41598-017-14273-4
25. Sajjadi, M., Javadi, M. H., Ashoorzadeh, Z., & Emami Niri, M. (2022). Economic optimization of enhanced geothermal systems using a fully analytical temperature profile. *Energy Sources, Part B*, *17*(1), Article 2101713. https://doi.org/10.1080/15567249.2022.2101713
26. Sanyal, S. K. (2000). Review of the state-of-the-art of numerical simulation of enhanced geothermal systems. *Geothermal Resources Council Transactions*, *24*, 181–186.
27. Sanyal, S. K., & Butler, S. J. (2005). An analysis of power generation prospects from enhanced geothermal systems. *Geothermal Resources Council Transactions*, *29*, 131–138.
28. Xue, Z., Ma, H., Wei, Y., Wu, W., Sun, Z., Chai, M., Zhang, C., & Chen, Z. (2024). Integrated technological and economic feasibility comparisons of enhanced geothermal systems associated with carbon storage. *Applied Energy*, *359*, Article 122757. https://doi.org/10.1016/j.apenergy.2024.122757
29. Zheng, J., Li, P., Dou, B., Fan, T., Tian, H., & Lai, X. (2022). Impact research of well layout schemes and fracture parameters on heat production performance of enhanced geothermal system considering water cooling effect. *Energy*, *255*, Article 124496. https://doi.org/10.1016/j.energy.2022.124496
30. Zhou, D., Tatomir, A., Niemi, A., Tsang, C.-F., & Sauter, M. (2022). Study on the influence of randomly distributed fracture aperture in a fracture network on heat production from an enhanced geothermal system (EGS). *Energy*, *250*, Article 123781. https://doi.org/10.1016/j.energy.2022.123781